JOURNAL OF GUIDANCE, CONTROL, AND DYNAMICS
Vol. 32, No. 4, July–August 2009

Libration Control of Electrodynamic Tethers Using Predictive Control with Time-Delayed Feedback

Paul Williams*
Delft University of Technology, 2926 HS Delft, The Netherlands

DOI: 10.2514/1.41039

One of the key problems for electrodynamic tethers is stabilization of the librational motion. In the case of a constant current in a circular orbit, an electrodynamic tether exhibits periodic solutions that are unstable, with the instability growing with the level of applied current. This paper proposes a new feedback control scheme that is capable of stabilizing the librational dynamics of electrodynamic tethers using only modulations in the electric current. The feedback does not require knowledge of the reference periodic solution, and as such, stabilizes the tether during orbital transfers. The feedback controller is based on a time-delayed predictive control law, which chooses the electric current at the current sampling time to minimize the predicted librations of the tether from the librations that were measured during the previous orbit. The control law is fully nonlinear and demonstrates convergence from large disturbances from the known periodic solution. Numerical results are presented that demonstrate its applicability when the orbit of the tether system is changing over time. In particular, the control law is able to handle both circular and elliptical orbits, as well as deorbit in the presence of a tilted, rotating magnetic field.

Nomenclature

a	=	orbit semimajor axis
$\mathbf{B}$	=	magnetic field vector in orbital frame (B_x, B_y, B_z)
e	=	orbit eccentricity
f_h	=	Lorentz force normal to the orbital plane
f_r	=	Lorentz force along radial direction
f_t	=	Lorentz force tangential to orbit
I	=	electric current
i	=	orbit inclination
L	=	UKF parameter
l	=	tether length
m	=	total system mass, $m_1 + m_2 + m_t$
m_1	=	main satellite mass
m_2	=	ballast mass
m_t	=	tether mass
m^*	=	reduced system mass
N	=	degree of discretization in predictive controller
$\mathbf{P}_k$	=	state covariance at kth sample
$\mathbf{P}_k^{xy}$	=	state cross covariance at kth sample
$\mathbf{P}_k^{yy}$	=	innovation covariance at kth sample
p	=	orbit semilatus rectum
$\mathbf{Q}$	=	state weighting in predictive controller
$\mathcal{Q}$	=	discrete noise covariance in unscented Kalman filter
Q_θ	=	generalized in-plane torque due to electrodynamic forces
Q_ϕ	=	generalized torque out-of-plane torque due to electrodynamic forces
R	=	control weighting in predictive controller
r	=	orbit radius
T	=	prediction time in predictive controller
T_p	=	period for sampling previous state
$\mathcal{X}$	=	sigma points in unscented Kalman filter
$\mathbf{y}_k$	=	predicted observation at kth sample
α	=	unscented Kalman filter scaling parameter
α_m	=	right ascension of magnetic field axis
β	=	unscented Kalman filter scaling parameter
β_m	=	tilt of magnetic field dipole from Earth's rotational axis
ε	=	nondimensional current
θ	=	in-plane libration angle
κ	=	unscented Kalman filter scaling parameter
λ	=	magnetic longitude parameter, $\alpha_m + \theta_s(t) - \Omega$
λ_s	=	unscented Kalman filter scaling parameter
μ	=	Earth's gravitational parameter
μ_m	=	magnetic field strength
ν	=	orbit true anomaly
ϖ	=	argument of perigee
ϕ	=	out-of-plane libration angle
Ω	=	right ascension of ascending node
ω	=	orbit angular velocity

Received 16 September 2008; revision received 30 December 2008; accepted for publication 3 January 2009.

*Applied Researcher, Faculty of Aerospace Engineering; tethered.systems@gmail.com. Member AIAA.

I. Introduction

TETHERED satellite systems have been flown successfully in space on a number of occasions. The potential for tethered satellite systems to provide exciting alternatives to conventional rocket propulsion [1,2] has seen a large amount of research undertaken to develop the technology. Tethered aerobraking [3], electrodynamic reboost of decaying orbits [4], and momentum transfer [5–7] are just some of the concepts being explored in the literature.

Particular interest has been shown in electrodynamic tethers for a variety of applications. Electrodynamic tethers are expected to be a viable and efficient means for generating power or controlling the orbit of future spacecraft [8–12]. Ishige et al. [13] studied the possibility of using an electrodynamic tether system for debris mitigation by maneuvering an electrodynamic tether system to rendezvous with debris, deploying the captured debris with the tether, and then changing the system orbit so that the debris can be safely released on a reentry trajectory. Strategies for maneuvering the system using simple trigonometric functions of the argument of latitude were presented. Yamagiwa et al. [14] studied the performance of an electrodynamic tether for changing the orbital altitude of a spacecraft with a hanging tether. Comparisons in terms of mission times for orbital transfers on different inclination orbits were performed with an ion thruster. They concluded that the electrodynamic tether concept is less useful if the inclination is greater than about 30 deg. However, this does not take into account more general orbital maneuvers or other system configurations. Lanoix et al. [15] studied the effect of both insulated and bare tethers for deorbiting applications. They assumed that the tether remains straight in their analysis, but is allowed to extend longitudinally, and used a simple

control law to help stabilize the tether librations. The control current is the superposition of a constant current for deorbit and a current that varies with the in-plane libration angle. Tragesser and San [16] developed a guidance algorithm for maneuvering hanging electrodynamic tethers between arbitrary orbits (restricted, however, to nonzero eccentricities because of the restrictions imposed by the perturbation equations). In their approach, the tether librations were neglected and control of the orbital elements was achieved by determining the variation in current to produce secular changes in each of the orbital elements. A total control law was constructed by a linear combination of the individual control laws and solving for the combination of coefficients to give the desired change in the orbital elements. To account for possible restrictions on current levels, the time of flight was adjusted to keep the current within the required bounds. The technique works reasonably well, with some small residual errors in the orbital elements caused by neglecting the periodic effects in the orbital elements. A more general set of control laws for spinning electrodynamic tethers was presented by Williams [17,18] who showed that a spinning electrodynamic tether system more efficiently maneuvers a system between different orbits. Williams [19] also used direct transcription to solve an optimal orbit boost/deboost problem with a librating tether. In this case, the variation in orbital parameters is not secular and the tether librations were shown to be beneficial because they allow greater components of the electrodynamic force to be directed along the velocity vector. Pearson et al. [20] summarized a proposed concept for an electrodynamic tether-driven spacecraft called the electrodynamic delivery express whose purpose is to deliver multiple small satellites from low Earth orbit (LEO) to different LEO orbits without expending propellant. They studied both hanging and spinning tether configurations for performing orbital maneuvers, and concluded that spinning tethers offer advantages from the point of view of efficiency and stability of the tether lateral modes [21]. Control of the tether flexible modes is achieved by superimposing an additional electromagnetic force (EMF) over the drive EMF to suppress the unwanted lateral vibration modes.

For cases where the tether current is not explicitly controlled for orbital maneuvering, the long-term dynamic behavior of the tether librations must be controlled. The control of electrodynamic tethers on inclined orbits is important because of the inherent instability provided by the electric current [22]. It has been conclusively established that, even for a tether modeled as an inelastic rod, the variation in electrodynamic forces over an orbit causes an influx of energy into the libration dynamics. Although, for the most part, the instability is slow to develop, it must be controlled for long-term operations. There exists a unique libration cycle, however, for which the net energy input per orbit is zero. Such a libration cycle is a periodic solution to the equations of motion for the system [23]. The periodic solution is unstable, with instability growing with the electric current [22]. For the case of a constant reference current, Williams [24] used an energy rate feedback approach to stabilize the librational motion of the tether around the periodic solution by adjusting the amount of current flowing in the tether. The drawback of this technique is that it requires a priori knowledge of the reference trajectory.

The idea of using time-delayed feedback for stabilizing unstable periodic orbits was analyzed by Bleich and Socolar [25], and applied to the pitch control of a gravity-gradient satellite in an elliptic orbit by Fujii et al. [26]. The approach was extended to electrodynamic tethers, which involves 2 degrees of freedom instead of 1, by Pelaez and Lorenzini [27], who assumed independent actuators for controlling the in- and out-of-plane librations. More recently, Inarrea and Pelaez [28] extended the previous work on time-delayed feedback control for electrodynamic tethers, but also assumed independent actuators in the in- and out-of-plane directions to help stabilize the electrodynamic tether around the periodic solution. The time-delayed feedback approach does not require knowledge of the periodic solution, but is limited by the practicality of having to use separate controllers for each degree of freedom. All of the libration stabilization schemes for the periodic solutions considered to date have considered frozen reference orbits (i.e., the orbit of the center of mass remains circular with constant inclination). Other control schemes such as those based on current switching schemes [29] do not provide the same level of efficiency for orbital maneuvering as schemes that can stabilize the periodic solution.

This paper develops a librational control algorithm for electrodynamic tethers using model predictive control. This approach enables control of the tether using only the electric current. Furthermore, by combining model predictive control with time-delayed feedback, it is possible to implement the controller without any predetermined reference trajectories. The controller is simulated for cases where the orbital inclination changes over time, as well as time-varying orbit eccentricity. The results show that the tether librations remain bounded and follow closely a periodic solution.

II. Mathematical Model

The electrodynamic tether system is modeled using the so-called dumbbell model in this paper. The dumbbell model treats the tether as inelastic and inflexible. The dumbbell model has been widely used in studies of tether dynamics and control [24–36]. Ultimately, any control law needs to be tested in a simulation model that best approximates the real system. In [37], it was shown that the superposition of control laws for the librational and flexible motion can be used to stabilize the motion of an electrodynamic tether. Williams in [37] uses the energy rate technique developed in [24] in two parts: the motion of the subsatellite is used to feed the librational energy feedback terms, whereas a point close to the tether attachment point (tether tangent) is used to represent the tether oscillation energy. Hence, in this work, focus is placed upon the librational motion only.

A representation of the mathematical model and the coordinates used to describe the motion is given in Fig. 1. The center of mass of the system is assumed to be in an orbit described by the orbit radius r and the true anomaly ν. The tether motion is described in the local orbital coordinate frame $Oxyz$, attached to the system center of mass at O. The orientation of the tether system is described by the spherical coordinates θ and ϕ, where θ is the in-plane tether libration angle, and ϕ is the out-of-plane tether libration angle. The tether length is denoted by l.

The main satellite from which the tether is deployed is m_1, and the subsatellite or ballast mass used to help stabilize the tether via the gravity gradient is m_2. The tether mass is assumed to be uniform along its length with mass density ρ. The total tether mass is given by m_t, and the total system mass is m.

A. Electrodynamic Tether Equations

The rotational kinetic energy of the tether is calculated in the tether body frame via

$$\mathcal{T} = \tfrac{1}{2}\omega^T[\mathbf{I}]\omega \tag{1}$$

where ω is the angular velocity vector of the tether in the body frame given by

$$\omega = (\dot{\theta} + \dot{\nu})\sin\phi\mathbf{i}_b - \dot{\phi}\mathbf{j}_b + (\dot{\theta} + \dot{\nu})\cos\phi\mathbf{k}_b \tag{2}$$

and $\mathbf{I}$ is the inertia tensor of the tether about the center of mass given by

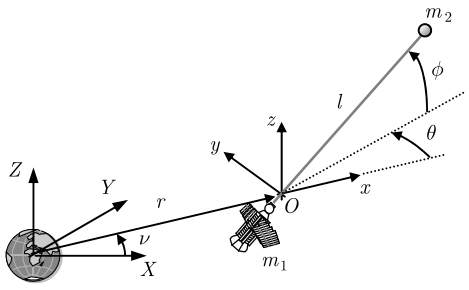

Fig. 1 Three-dimensional electrodynamic tether dumbbell model.

$$\mathbf{I} = \text{diag}[0, I_{\text{cm}}, I_{\text{cm}}] \tag{3}$$

where

$$I_{\text{cm}} = m_1 s_1^2 + m_2 s_2^2 + \int_{-s_1}^{s_2} \rho s^2 \text{d}s \tag{4}$$

with

$$s_1 = \left(m_2 + \frac{m_t}{2}\right) l/m \tag{5}$$

$$s_2 = \left(m_1 + \frac{m_t}{2}\right) l/m \tag{6}$$

The moment of inertia of the system about the center of mass can be expressed in the simplified form

$$I_{\text{cm}} = \left[\frac{(m_1 + \frac{m_t}{2})(m_2 + \frac{m_t}{2})}{m} - \frac{m_t}{6}\right] l^2 = m^* l^2 \tag{7}$$

where m^* is defined as the reduced mass of the system.

The kinetic energy of the system is given by

$$\mathcal{T} = \tfrac{1}{2} m^* l^2 [\dot{\phi}^2 + (\dot{\theta} + \dot{\nu})^2 \cos^2\phi] \tag{8}$$

The potential energy for the system configuration under consideration consists only of the gravity potential due to a spherical central planet. For tethers of moderate length, the following binomial expansion for the gravitational potential energy can be used:

$$\mathcal{V} = -\frac{\mu m}{r} + \frac{\mu m^* l^2}{2r^3}(1 - 3\cos^2\theta\cos^2\phi) \tag{9}$$

Direct application of Lagrange's equations yields the equations of motion for the tether librational dynamics. After changing the independent variable from time to the orbit true anomaly, the following equations are obtained:

$$\theta'' = 2(\theta' + 1)\left[\frac{e\sin\nu}{1 + e\cos\nu} + \phi' \tan\phi\right] - \frac{3}{1 + e\cos\nu}\sin\theta\cos\theta + \frac{Q_\theta}{m^* l^2 \omega^2 \cos^2\phi} \tag{10}$$

$$\phi'' = \frac{2e\sin\nu}{1 + e\cos\nu}\phi' - \left[(\theta' + 1)^2 + \frac{3}{1 + e\cos\nu}\cos^2\theta\right]\sin\phi\cos\phi + \frac{Q_\phi}{m^* l^2 \omega^2} \tag{11}$$

where e is the orbit eccentricity. Note that the coupling between the tether librations and the orbit of the center of mass is not included in these equations. The right-hand sides of Eqs. (10) and (11) contain the torques due to electrodynamic forces. These are evaluated using the principle of virtual work as follows:

$$Q_{q_j} = \int_m \mathbf{F} \cdot \frac{\partial \mathbf{R}_m}{\partial q_j} \tag{12}$$

where $\mathbf{F}$ is the vector of external forces, $\mathbf{R}_m$ is the inertial vector to the line of action of the force $\mathbf{F}$ acting on the mth system mass, and q_j are the generalized coordinates.

Consider the force acting on a small element of the tether at a distance s from the center of mass (measured positively toward m_2). The elemental Lorentz force is given by

$$d\mathbf{F} = I(s)(\mathbf{t} \times \mathbf{B})\text{d}s \tag{13}$$

where $I(s)$ is the current in the tether, $\mathbf{t}$ is the unit vector tangent to the tether line in the direction of s, and $\mathbf{B}$ is the magnetic field vector measured at the center of mass of the system. It is assumed that the magnetic field is constant along the tether as in [23].

The calculation of the required vectors to evaluate the generalized forces is carried out in a rotating reference frame attached to the system center of mass. The unit vectors $\mathbf{i}$, $\mathbf{j}$, and $\mathbf{k}$ are introduced, which are aligned with the local vertical, local horizontal, and the orbit normal, respectively. The required vectors are given as follows:

$$\mathbf{t} = \cos\theta\cos\phi\mathbf{i} + \sin\theta\cos\phi\mathbf{j} + \sin\phi\mathbf{k} \tag{14}$$

$$\mathbf{R}(s) = (R + s\cos\theta\cos\phi)\mathbf{i} + s\sin\theta\cos\phi\mathbf{j} + s\sin\phi\mathbf{k} \tag{15}$$

$$\mathbf{B} = B_x\mathbf{i} + B_y\mathbf{j} + B_z\mathbf{k} \tag{16}$$

The generalized electromagnetic forces can now be evaluated as

$$Q_{q_j} = \int_{-s_1}^{s_2} \text{d}\mathbf{F} \cdot \frac{\partial \mathbf{R}}{\partial q_j} = \int_{-s_1}^{s_2} I(s)(\mathbf{t} \times \mathbf{B}) \cdot \frac{\partial \mathbf{R}}{\partial q_j}\text{d}s \tag{17}$$

$$Q_\theta = \cos\phi[\sin\phi(B_x\cos\theta + B_y\sin\theta) - B_z\cos\phi]\int_{-s_1}^{s_2} I(s)s\text{d}s = \frac{\bar{I} l^2}{2}\Lambda\cos\phi[\sin\phi(B_x\cos\theta + B_y\sin\theta) - B_z\cos\phi] \tag{18}$$

$$Q_\phi = [B_y\cos\theta - B_x\sin\theta]\int_{-s_1}^{s_2} I(s)s\text{d}s = \frac{\bar{I} l^2}{2}\Lambda[B_y\cos\theta - B_x\sin\theta] \tag{19}$$

where $\Lambda = (m_1 - m_2)/m$, and the overbar on the electric current refers to the fact that we are assuming the current is uniform along the tether.

For the case of a tilted dipole model of the Earth's magnetic field, the components of the magnetic field B_x, B_y, and B_z can be evaluated (see the Appendix). Substitution of Eqs. (A4–A6) into Eqs. (10) and (11), and using the relationship that $\mu/r^3 = \omega^2/(1 + e\cos\nu)$ yields the general form of the equations of motion

$$\begin{aligned}\theta'' = {} & 2(\theta' + 1)\left[\frac{e\sin\nu}{1 + e\cos\nu} + \phi'\tan\phi\right] - \frac{3}{1 + e\cos\nu}\sin\theta\cos\theta \\ & + \frac{\varepsilon}{1 + e\cos\nu}[\tan\phi(-2\sin(\varpi + \nu)\sin i\cos\beta_m\cos\theta \\ & - 2\sin\beta_m\{\cos\lambda\cos(\varpi + \nu) + \sin\lambda\sin(\varpi + \nu)\cos i\}\cos\theta \\ & + \cos(\varpi + \nu)\sin i\cos\beta_m\sin\theta - \sin\beta_m\{\cos\lambda\sin(\varpi + \nu) \\ & - \sin\lambda\cos(\varpi + \nu)\cos i\}\sin\theta) - \cos i\cos\beta_m \\ & + \sin\beta_m\sin i\sin\lambda]\end{aligned} \tag{20}$$

$$\begin{aligned}\phi'' = {} & \frac{2e\sin\nu}{1 + e\cos\nu}\phi' - \left[(\theta' + 1)^2 + \frac{3}{1 + e\cos\nu}\cos^2\theta\right]\sin\phi\cos\phi \\ & + \frac{\varepsilon}{1 + e\cos\nu}[\cos(\varpi + \nu)\sin i\cos\beta_m\cos\theta \\ & - \sin\beta_m\{\cos\lambda\sin(\varpi + \nu) - \sin\lambda\cos(\varpi + \nu)\cos i\}\cos\theta \\ & + 2\sin(\varpi + \nu)\sin i\cos\beta_m\sin\theta + 2\sin\beta_m\{\cos\lambda\cos(\varpi + \nu) \\ & + \sin\lambda\sin(\varpi + \nu)\cos i\}\sin\theta]\end{aligned} \tag{21}$$

where

$$\varepsilon = \frac{\mu_m \int_{-s_1}^{s_2} I(s)s\text{d}s}{\mu m^* l^2} = \Phi_m \frac{\bar{I}\mu_m}{\mu} \tag{22}$$

The parameter Φ_m is defined by

$$\Phi_m = \frac{\Lambda}{2m^*} = \frac{1}{2}\frac{m_1 - m_2}{(m_1 + m_t/3)(m_2 + m_t/3) - m_t^2/36} \tag{23}$$

In the case where the main satellite's mass is very large compared to the tether and subsatellite, the orbit is often assumed fixed and Eq. (23) simplifies to

$$\Phi_m = \frac{1}{2(m_2 + m_t/3)} \tag{24}$$

which is the parameter defined in the work on periodic solutions by Pelaez and Lara [23]. In the case of equal end masses and a uniform current, the torque due to electrodynamic forces is zero. For nonuniform currents, Eq. (22) must be used and the integral of the current must be evaluated numerically. By properly distributing the mass of the system it is possible to achieve "self-balancing" to reduce the instability due to the electric current [38].

B. Effects of Electrodynamic Forces on Center-of-Mass Orbit

Previous control laws for stabilizing the periodic solutions [24–28] have been derived and simulated using unperturbed tether dynamics. However, because one of the future applications of electrodynamic tether systems is likely to be orbital maneuvering, it is important to assess the effects of varying orbital parameters on the stability of the controller. In this paper, the effects of a decaying orbit are taken into consideration by using the general perturbation equations. In Gauss's form, they are given by

$$\dot{a} = (2a^2/h)[e\sin(\nu)f_r + (p/r)f_t] \tag{25}$$

$$\dot{e} = (1/h)\{p\sin(\nu)f_r + [(p + r)\cos(\nu) + re]f_t\} \tag{26}$$

$$\dot{\varpi} = \left(\frac{1}{he}\right)[-p\cos(\nu)f_r + (p + r)\sin(\nu)f_t] - (r\sin(\varpi + \nu)\cos i/h\sin i)f_h \tag{27}$$

$$\dot{i} = (r\cos(\varpi + \nu)/h)f_h \tag{28}$$

$$\dot{\Omega} = (r\sin(\varpi + \nu)/h\sin i)f_h \tag{29}$$

$$\dot{\nu} = h/r^2 + (1/eh)[p\cos(\nu)f_r - (p + r)\sin(\nu)f_t] \tag{30}$$

where a is the orbit semimajor axis, $h = \sqrt{\mu a(1 - e^2)}$ is the orbit angular momentum, ϖ is the argument of perigee, $p = a(1 - e^2)$ is the semilatus rectum, r is the orbit radius, Ω is the right ascension of the ascending node, i is the orbit inclination, and f_r, f_t, and f_h are the components of the disturbing acceleration vector in the radial, transverse, and orbit normal directions, respectively,

$$f_r = \frac{Il}{m}(B_z\sin\theta\cos\phi - B_y\sin\phi) \tag{31}$$

$$f_t = \frac{Il}{m}(B_x\sin\phi - B_z\cos\theta\cos\phi) \tag{32}$$

$$f_h = \frac{Il}{m}(B_y\cos\theta\cos\phi - B_x\sin\theta\cos\phi) \tag{33}$$

Note that Gauss's form of the general perturbation equations contains singularities for zero eccentricity and zero inclination. It is possible to avoid these singularities by using a set of modified equinoctial elements [39]. However, for simplicity, Eqs. (25–30) will be used.

III. Nonlinear Predictive Control Design

In this section, the fundamental approach used to design the libration controller is presented. The approach is based on predictive or receding horizon control. The fundamental premise of a predictive control methodology is to use a model or representation of the system to be controlled to simulate the system forward in time from the current time. The control input over the future time horizon is optimized to minimize a suitable cost function, which is usually a function of the control signal. Typical cost functions are quadratic in the states and controls, but this need not be the case.

Most of the model predictive control strategies that have been suggested are based on low-order discretizations of the system dynamics, such as Euler integration. Recently, Dunbar et al. [40] and Franz et al. [41] applied receding horizon control to the Caltech ducted fan (an indoor, tethered flight control experiment with dynamics similar to the longitudinal dynamics of an aircraft) based on a B-spline parameterization of the trajectories. In recent years, pseudospectral methods, and, in particular, the Legendre pseudospectral method [42,43], have been used for real-time generation of optimal trajectories for many systems [44–48]. The traditional approach discretizes the dynamics via differentiation operators applied to expansions of the states in terms of Lagrange polynomial bases. Another approach is to discretize the dynamics via Gauss–Lobatto quadratures. The approach has been more fully described by Williams [49] and in explicit form for fifth-order polynomials in [50] and the main details are given in the following section. It should be noted that Benson [51] used a similar approach based on Gaussian quadrature. The main difference between the two approaches is that the Gauss–Lobatto approach gives the controls explicitly at the initial time, which is necessary for real-time optimal control.

A. Discretization Approach

Instead of presenting a general approach to solving optimal control problems, the Gauss–Lobatto approach presented in this section is restricted to the form of the problem solved here. The goal is to find the state and control history $\{\mathbf{x}(t), \mathbf{u}(t)\}$ to minimize the cost function

$$\mathcal{J} = \mathcal{M}[\mathbf{x}(t + T)] + \int_t^{t+T} \mathcal{L}[\mathbf{x}(t^*), \mathbf{u}(t^*), t^*]\mathrm{d}t^* \tag{34}$$

subject to the nonlinear state equations

$$\dot{\mathbf{x}}(t) = \mathbf{f}[\mathbf{x}(t), \mathbf{u}(t), t] \tag{35}$$

the initial and terminal constraints

$$\psi_0[\mathbf{x}(t)] = \mathbf{0} \tag{36}$$

$$\psi_f[\mathbf{x}(t + T)] = \mathbf{0} \tag{37}$$

the mixed state-control path constraints

$$\mathbf{g}_L \le \mathbf{g}[\mathbf{x}(t), \mathbf{u}(t), t] \le \mathbf{g}_U \tag{38}$$

and the box constraints

$$\mathbf{x}_L \le \mathbf{x}(t) \le \mathbf{x}_U, \qquad \mathbf{u}_L \le \mathbf{u}(t) \le \mathbf{u}_U \tag{39}$$

where $\mathbf{x} \in \mathbb{R}^{n_x}$ are the state variables, $\mathbf{u} \in \mathbb{R}^{n_u}$ are the control inputs, $t \in \mathbb{R}$ is the time, $\mathcal{M}$: $\mathbb{R}^{n_x} \times \mathbb{R} \to \mathbb{R}$ is the Mayer component of the cost function, that is, the terminal, nonintegral cost in Eq. (34), $\mathcal{L}$: $\mathbb{R}^{n_x} \times \mathbb{R}^{n_u} \times \mathbb{R} \to \mathbb{R}$ is the Bolza component of the cost function, that is, the integral cost in Eq. (34), $\psi_0 \in \mathbb{R}^{n_x} \times \mathbb{R} \to \mathbb{R}^{n_0}$ are the initial point conditions, $\psi_f \in \mathbb{R}^{n_x} \times \mathbb{R} \to \mathbb{R}^{n_f}$ are the final point conditions, and $\mathbf{g}_L \in \mathbb{R}^{n_x} \times \mathbb{R}^{n_u} \times \mathbb{R} \to \mathbb{R}^{n_g}$ and $\mathbf{g}_U \in \mathbb{R}^{n_x} \times \mathbb{R}^{n_u} \times \mathbb{R} \to \mathbb{R}^{n_g}$ are the lower and upper bounds on the path constraints.

The basic idea behind the Gauss–Lobatto quadrature discretization is to approximate the vector field by an Nth degree Lagrange interpolating polynomial

$$\mathbf{f}(t) \approx \mathbf{f}_N(t) \tag{40}$$

expanded using values of the vector field at the set of Legendre–Gauss–Lobatto (LGL) points. The LGL points are defined on the interval $\tau \in [-1, 1]$ and correspond to the zeros of the derivative of the Nth degree Legendre polynomial, $L_N(\tau)$, as well as the end points -1 and 1. The computation time is related to the time domain by the transformation

$$t = \frac{T}{2}\tau + \frac{T}{2} \tag{41}$$

The Lagrange interpolating polynomials are written as

$$\mathbf{f}_N(t) = \sum_{k=0}^{N} \mathbf{f}_k \phi_k(\tau) \tag{42}$$

where $t = t(\tau)$ because of the shift in the computational domain. The Lagrange polynomials may be expressed in terms of the Legendre polynomials as

$$\phi_k(\tau) = \frac{(\tau^2 - 1)L_N'(\tau)}{(\tau - \tau_k)N(N+1)L_N(\tau_k)}, \qquad k = 0, \ldots, N \tag{43}$$

Approximations to the state equations are obtained by integrating Eq. (42),

$$\mathbf{x}_k = \mathbf{x}_0 + \frac{T}{2}\int_{-1}^{1} \sum_{j=0}^{N} \phi_j(\tau)\mathbf{f}(t_j)\mathrm{d}\tau, \qquad k = 1, \ldots, N \tag{44}$$

Equation (44) can be rewritten in the form of Gauss–Lobatto quadrature approximations as

$$\mathbf{x}_k = \mathbf{x}_0 + \frac{T}{2}\sum_{j=0}^{N} \mathcal{I}_{k-1,j}\mathbf{f}(t_j), \qquad k = 1, \ldots, N \tag{45}$$

where the entries of the $N \times (N+1)$ integration matrix $\mathcal{I}$ are derived by Williams [49]. The cost function is approximated via a full Gauss–Lobatto quadrature as

$$\mathcal{J}_N = \mathcal{M}[\mathbf{x}_N] + \frac{T}{2}\sum_{j=0}^{N} \mathcal{L}[\mathbf{x}_j, \mathbf{u}_j, t_j]w_j \tag{46}$$

Thus the discrete states and controls at the LGL points $(\mathbf{x}_0, \ldots, \mathbf{x}_N, \mathbf{u}_0, \ldots, \mathbf{u}_N)$ are the optimization parameters, which means that the path constraints and box constraints are easily enforced. The continuous problem has been converted into a large-scale parameter optimization problem. The resulting nonlinear programming problem is solved using SNOPT [52] in this work. The specific implementation is considered in the following section. In all cases analytic Jacobians of the cost and discretized equations of motion are provided to SNOPT. These may be computed relatively easily for the current discretization, as well as Legendre pseudospectral discretizations, and is not true of many other possible discretizations.

B. Time-Delayed Predictive Control

The above methodology is capable of tracking time-varying reference solutions and stabilizing systems around particular set points. This capability will be demonstrated in the numerical results section. However, the drawback of this in its current form is that it relies on knowledge of a suitable reference solution. As pointed out earlier, the tether dumbbell model exhibits periodic solutions when the Earth's magnetic field is modeled as a nontilted dipole. Although this could be used as a reference, it implies knowledge of the periodic solution, or requires that the periodic solution be generated in real time. This is not a desirable requirement particularly because such solutions are only approximate when dealing with a real system in the presence of a tilted magnetic field.

This apparent difficulty is circumvented in this paper by a novel control approach that will be termed "time-delayed predictive control." Note that this is not a standard term, but has been coined to describe the work presented in this paper. Consider the example where the system dynamics are observable, and the motion of the system over the previous orbit is defined by

$$\mathbf{x}^-(t) := \mathbf{x}(t - T_p), \qquad t \in [t_0, t_0 + T_p] \tag{47}$$

where T_p is the period of the orbit. The state for the electrodynamic tether system is defined as $\mathbf{x} \triangleq [\theta, \theta', \phi, \phi']$. In a real system, the right-hand side of Eq. (47) is replaced by a filtered state estimate. Furthermore, the desired electric current to achieve the mission objectives is defined by

$$\mathbf{u}(t) := \mathbf{u}_d(t), \qquad t \in [t_0, t_0 + T] \tag{48}$$

The control input at the current time t is selected so as to minimize the combination of the deviation of the system response from the response measured during the previous orbit, and the deviation of the control input from the desired control input,

$$\mathcal{J} = \int_t^{t+kT} [(\mathbf{x}(t) - \mathbf{x}^-(t))^T \mathbf{Q}(\mathbf{x}(t) - \mathbf{x}^-(t)) + (\mathbf{u}(t) - \mathbf{u}_d(t))^T \mathbf{R}(\mathbf{u}(t) - \mathbf{u}_d(t))]\mathrm{d}t \tag{49}$$

where $\mathbf{Q}$ and $\mathbf{R}$ are state and control weighting matrices, respectively, and $k \in [0, 1]$ is the fraction of the orbital period to predict ahead. This cost must be minimized subject to the dynamical constraints given by Eq. (35), with the initial conditions

$$\mathbf{x}(t) = \mathbf{x}^-(t_0 + T_p) \tag{50}$$

as well as the control constraints

$$\delta\mathbf{u}_{\min} \le \mathbf{u}(t) - \mathbf{u}_d(t) \le \delta\mathbf{u}_{\max} \tag{51}$$

Note that in this formulation, no terminal constraints are used to allow more freedom for the solution to adjust to perturbations and changes in the magnetic field vector. The structure of the controller designed using this approach is summarized in Fig. 2.

C. Nonlinear State Estimation

One of the limitations of the control scheme outlined in the previous section is that it relies on full state feedback. However, it should be remarked that this is true of almost all proposed feedback controllers for electrodynamic tethers. The problem with this assumption is that the control algorithms may be susceptible to measurement and observer noise. For example, some schemes could diverge if the exact tether states are not known. Furthermore, digitization of the control signal and time delays in the system are other factors that are often neglected. Although time delays are likely to be very small compared to the time scales involved, it is necessary to consider measurement noise and observer design to properly validate controllers.

In this section, a nonlinear observer is designed to estimate the tether librations and libration rates using position measurements of the tether end body. No specific sensors are considered here, but it is conceivable that Global Positioning System positions of the satellite and ballast mass could be used to form estimates of the tether state for systems in low Earth orbit.

D. Tether Libration State Estimation

Consider the problem where the positions of the two end bodies of the tethered system are measured in the orbital coordinate system. Assume then that the measurements are available in the form of the differences in the position vector, that is,

$$y_1 = X_2 - X_1 = l\cos\theta\cos\phi \qquad y_2 = Y_2 - Y_1 = l\sin\theta\cos\phi$$
$$y_3 = Z_2 - Z_1 = l\sin\phi \tag{52}$$

The goal of the state estimation process is to use the measurements of the two end bodies, which will contain noise, to estimate the full state

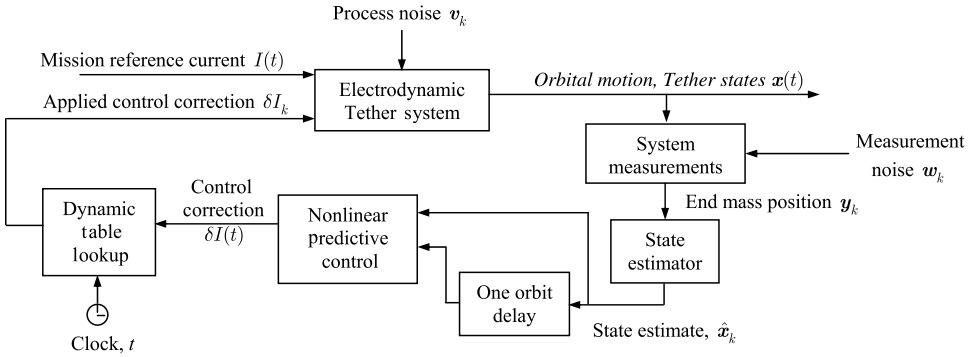

Fig. 2 Control structure for electrodynamic tether libration stabilization.

vector consisting of θ, θ', ϕ, and ϕ'. The filtering process is undertaken using the unscented Kalman filter, as described in the following section. Note that throughout this paper, it is assumed that the orbital elements of the system are determined using a different subsystem and are fed into the librational control system. As such, no formal consideration is given to the problem of orbit determination for the electrodynamic tether system.

E. Unscented Kalman filtering

The unscented Kalman filter (UKF) was developed by Julier and Uhlmann [53]. It is called the UKF because it is based on the unscented transformation, which is a technique for calculating the statistics of a random variable undergoing a nonlinear transformation, and does not require the computation of the Jacobian or Hessian matrices. The UKF assumes a discrete time process model of the form

$$\mathbf{x}_{k+1} = \mathbf{f}(\mathbf{x}_k, \mathbf{u}_k, \mathbf{v}_k, t_k) \tag{53}$$

$$\mathbf{y}_k = \mathbf{h}(\mathbf{x}_k, \mathbf{u}_k, \mathbf{w}_k, t_k) \tag{54}$$

where $\mathbf{x}_k \in \mathbb{R}^{n_x}$ is the system state vector, $\mathbf{u}_k \in \mathbb{R}^{n_u}$ is the system control input, $\mathbf{y}_k \in \mathbb{R}^{n_y}$ is the system measurement vector, $\mathbf{v}_k \in \mathbb{R}^{n_v}$ is the vector of process noise, assumed to be white Gaussian with zero mean and covariance $\mathbf{Q}_k \in \mathbb{R}^{n_v \times n_v}$, $\mathbf{w}_k \in \mathbb{R}^{n_w}$ is a vector of measurement noise, assumed to be white Gaussian with zero mean and covariance $\mathbf{R}_k \in \mathbb{R}^{n_w \times n_w}$. For the results in this paper, the continuous system is converted to a discrete system by means of a fourth-order Runge–Kutta method.

In the following, the process and measurement noise are implicitly augmented with the state vector as follows

$$\mathbf{x}_k^a = \begin{bmatrix} \mathbf{x}_k \\ \mathbf{v}_k \\ \mathbf{w}_k \end{bmatrix} \tag{55}$$

The first step in the filtering process is to compute the set of sigma points as follows:

$$\mathcal{X}_{k-1} = [\hat{\mathbf{x}}_{k-1}^a, \hat{\mathbf{x}}_{k-1}^a + \gamma\sqrt{\mathbf{P}_k}, \hat{\mathbf{x}}_{k-1}^a - \gamma\sqrt{\mathbf{P}_k}] \tag{56}$$

where $\hat{\mathbf{x}}^a$ is the mean estimate of the state vector, $\mathbf{P}_k$ is the covariance matrix, and the parameter γ is defined by

$$\gamma = \sqrt{L + \lambda_s} \tag{57}$$

$\lambda_s = \alpha^2(L + \kappa) - L$ is a scaling parameter, with the values of α and κ selected appropriately, and L is the size of the vector $\hat{\mathbf{x}}^a$. The sigma points are then propagated through the nonlinear dynamics as follows:

$$\mathcal{X}^*_{k|k-1} = \mathbf{f}(\mathcal{X}_{k-1}, \mathbf{u}_k, t_k) \tag{58}$$

The predicted mean for the state estimate is calculated from

$$\hat{\mathbf{x}}_k^- = \sum_{i=0}^{2L} W_i^{\text{mean}} \mathcal{X}^*_{i,k|k-1} \tag{59}$$

where

$$W_i^{\text{mean}} = \begin{cases} \frac{\lambda_s}{L+\lambda_s}, & i = 0 \\ \frac{1}{2(L+\lambda_s)}, & i = 1, \ldots, 2L \end{cases} \tag{60}$$

The covariance matrix is predicted forward by

$$\mathbf{P}_k^- = \sum_{i=0}^{2L} W_i^{\text{cov}} [\mathcal{X}^*_{i,k|k-1} - \hat{\mathbf{x}}_k^-][\mathcal{X}^*_{i,k|k-1} - \hat{\mathbf{x}}_k^-]^T \tag{61}$$

where

$$W_i^{\text{cov}} = \begin{cases} \frac{\lambda_s}{L+\lambda_s} + (1 - \alpha^2 + \beta), & i = 0 \\ \frac{1}{2(L+\lambda_s)}, & i = 1, \ldots, 2L \end{cases} \tag{62}$$

Next, the propagated sigma points are augmented by

$$\mathcal{X}_{k|k-1} = [\mathcal{X}^*_{k|k-1}, \mathcal{X}^*_{k|k-1} + \gamma\sqrt{\mathbf{Q}_k}, \mathcal{X}^*_{k|k-1} - \gamma\sqrt{\mathbf{Q}_k}] \tag{63}$$

The augmented sigma points are propagated through the measurement equations

$$\mathcal{Y}_{k|k-1} = \mathbf{h}(\mathcal{X}_{k|k-1}, \mathbf{u}_k, t_k) \tag{64}$$

The mean observation is obtained by

$$\hat{\mathbf{y}}_k^- = \sum_{i=0}^{2L} W_i^{\text{mean}} \mathcal{Y}_{i,k|k-1} \tag{65}$$

The output covariance is calculated using

$$\mathbf{P}_k^{yy} = \sum_{i=0}^{2L} W_i^{\text{cov}} [\mathcal{Y}_{i,k|k-1} - \hat{\mathbf{y}}_k^-][\mathcal{Y}_{i,k|k-1} - \hat{\mathbf{y}}_k^-]^T \tag{66}$$

The cross-correlation matrix is determined from

$$\mathbf{P}_k^{xy} = \sum_{i=0}^{2L} W_i^{\text{cov}} (\mathcal{X}_{i,k|k-1} - \hat{\mathbf{x}}_k^-)(\mathcal{Y}_{i,k|k-1} - \hat{\mathbf{y}}_k^-)^T \tag{67}$$

The gain for the Kalman update equations is computed from

$$\mathcal{K}_k = \mathbf{P}_k^{xy} (\mathbf{P}_k^{yy})^{-1} \tag{68}$$

The state estimate is updated with a measurement of the system $\mathbf{y}_k$ using

$$\hat{\mathbf{x}}_k = \hat{\mathbf{x}}_k^- + \mathcal{K}_k(\mathbf{y}_k - \hat{\mathbf{y}}_k^-) \tag{69}$$

and the covariance is updated using

$$\mathbf{P}_k^+ = \mathbf{P}_k^- - \mathcal{K}_k \mathbf{P}_k^{yy} \mathcal{K}_k^T \tag{70}$$

These equations are implemented together with the feedback controller in the examples to be presented in the following section. It should be noted that the measurement update defined in Eqs. (64–70) is only necessary when new measurement data are available.

IV. Numerical Results

Several numerical examples are presented in this section to show the effectiveness of the control and estimation architecture. As illustrated in Fig. 2, the most general form of the controller uses a state estimator in the feedback loop. However, in several examples, both observer-based feedback and true state feedback are used to compare performance. The first example demonstrates the ability of the predictive controller for tracking known reference trajectories. The second example illustrates the effect that imperfect state feedback has on the trajectory tracking controller. The third example shows the performance of the time-delayed feedback controller without any predetermined reference trajectory for tracking, for the case where the orbit remains circular. This is followed by application of the controller to an elliptic orbit, and finally to consider the cases where the orbit is continually changing in response to the applied current. The final example demonstrates the robustness of the controller for the practical case of deorbit with a nontilted dipole representing the Earth's magnetic field.

A. Reference Trajectory Tracking

To demonstrate the instability of the electrodynamic tether system under a constant current input, a system in a 45-deg inclination orbit is considered. The periodic solution for the case of a nontilted dipole is determined using the method presented in [54]. For a nondimensional current input of $\varepsilon = 1.5$ the periodic solution shown in Fig. 3a is obtained.

This periodic solution is unstable, as illustrated by perturbing the initial conditions as follows:

$$[\delta\theta, \delta\theta', \delta\phi, \delta\phi'] = [-0.04 \text{ rad}, -0.1, 0.05 \text{ rad}, 0.03] \tag{71}$$

Figure 3b illustrates a numerical simulation of the system with the initial conditions perturbed away from the periodic solution. Within three orbits, the periodic solution diverges completely and the tether begins rotating around its center of mass. The instability is a function of the current level, and smaller values of ε would take longer to diverge.

Application of the pure predictive tracking controller to the same problem is illustrated in Fig. 4a for a simulation time of 10 orbits. The controller is discretized using $N = 30$, which corresponds to a 31-deg polynomial. The horizon length is set equal to one-half an orbit, and the sampling time is equal to 0.1 rad. This equates to roughly 90 s for a low Earth orbit. In other words, the system is predicted forward by one-half an orbit each time the optimization is performed. Each optimization takes place every 0.1 rad increment in the true anomaly (90 s), with an average computation time of 0.45 s (min time= 0.20 s, max time = 0.66 s) on an Intel T2600 2.16 GHz running MATLAB R2008a. The control signal is implemented with a much finer sampling time, approximately 2 s. The control signal is interpolated using cubic splines to achieve a higher fidelity than can be achieved by linear interpolation. The control input is limited to the range $\varepsilon \in [0, 2]$ to prevent reversal of the current direction or excessive current draw. The weighting matrices for penalizing deviations from the reference trajectories are selected as $\mathbf{Q} = \mathbf{I}_{4\times4}$, and $R = 5$. In this example, the reference trajectories are known and

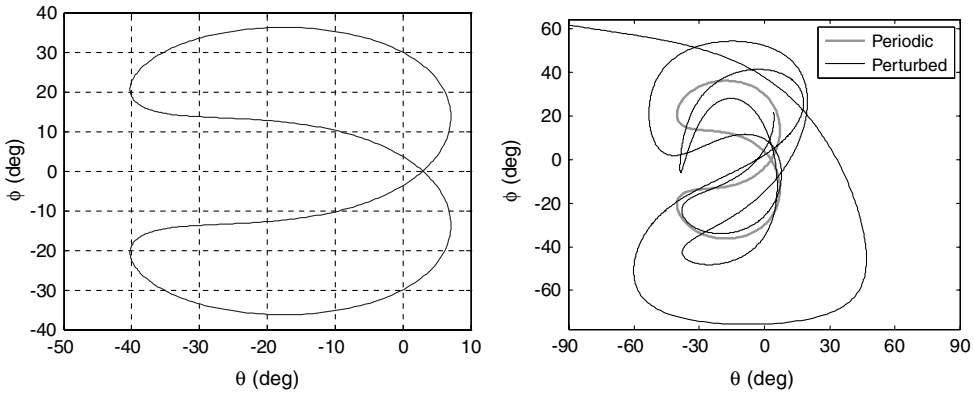

a) b)

Fig. 3 a) Periodic solution for electrodynamic tether in circular orbit with $\varepsilon = 1.5$; b) instability of open-loop periodic solution.

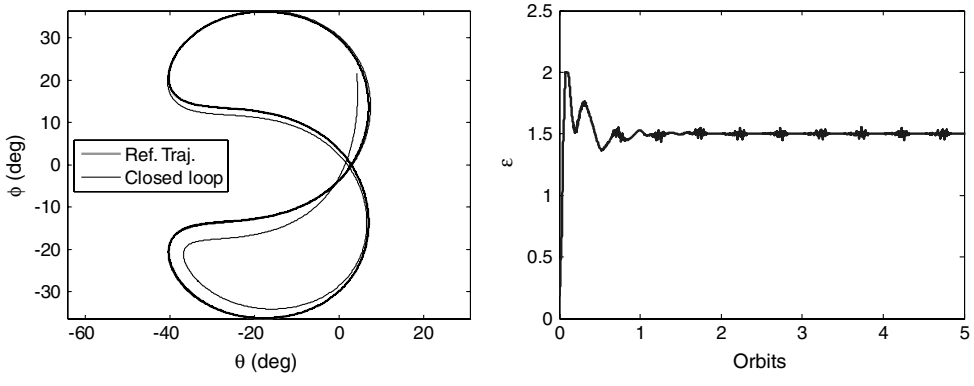

a) b)

Fig. 4 a) Convergence of predictive tracking controller for electrodynamic tether problem; b) applied nondimensional feedback control to track reference trajectory.

terminal constraints are employed to force the predicted trajectory to be equal to the reference trajectory at the end of the prediction horizon. It is important to point out that this example merely tracks a predetermined reference trajectory and is not an implementation of the time-delayed predictive control.

Figure 4a shows that the predictive controller is able to achieve convergence in approximately one orbit and maintains stable tracking. This should be contrasted with the case where no closed-loop control is provided in Fig. 3b. The variation in current required to track the trajectory is shown in Fig. 4b. There is initially a large variation in the current input due to the fact that terminal constraints are used to provide fast stabilization. Hence, regardless of the ratio of Q/R, the initial current must vary over a large range to meet the terminal constraints. The results also show some small noise in the current after the system has been stabilized around the reference trajectory. This can be attributed to the digitization of the reference trajectory. This noise can be reduced by providing a finer mesh for the reference trajectories. However, this is not the goal of this work.

B. State Estimation Implementation and Performance

The performance of the state estimator for the electrodynamic tether system is demonstrated in this section. The reference periodic solution is used to generate the system measurements. The discrete system process noise is defined by

$$\mathbf{Q}_{\theta} = 10^{-6}, \qquad \mathbf{Q}_{\theta'} = 10^{-3}, \qquad \mathbf{Q}_{\phi} = 10^{-6}, \qquad \mathbf{Q}_{\phi'} = 10^{-3} \tag{72}$$

and the measurement noise covariance is defined by

$$\mathbf{R} = \text{diag}[400, 400, 400]\ \text{m}^2 \tag{73}$$

which is applied to the measurements in the x, y, and z directions. The tether length is equal to 5 km, and filter predictions and measurement updates are set to occur at the same low frequency of approximately 0.2 Hz. In reality, faster updates are possible, but not required for the librational motion of the tether. The measurement noise is assumed to be Gaussian. Although this is unlikely to be the case in reality, the measurement noise covariance is set to be conservatively large [55], that is, standard deviations of 20 m in the three axes compared with typical errors between 1 and 10 m. The initial state estimate is assumed to be zero for all states, that is, far from the true solution. The initial covariance is chosen to reflect the fact that there is a large uncertainty in the initial state estimate,

$$\mathbf{P}_0 = \text{diag}[50^2\ \text{deg}^2, 50^2, 50^2\ \text{deg}^2, 50^2] \tag{74}$$

Results of the application of the unscented filter to the electrodynamic tether are shown in Fig. 5, with the unscented filter parameters selected as $\alpha = 0.5$, $\beta = 2$, and $\kappa = -1$. The results show that the state estimates converge very quickly to the true solution for all states. However, the results also illustrate that the initial uncertainty in the state estimate causes large initial transients in the estimates. For the control system, it is important that some time is given for the filter to converge before using the estimates. This could entail turning the filtering algorithm on before switching on the current for an electrodynamic tether. In the case of a bare tether, no feedback control should be applied before the filter converges to a reliable estimate. In practice, the true state of the system is not known so it may be difficult to judge true convergence. However, some measure of the filter covariance or innovation sequence can be used to judge convergence of the filter. Alternatively, a safe time window can be defined based on Monte Carlo analysis of the control system. In this paper, a time window is used based on the expected convergence rate of the filter. Typically, one orbit is more than sufficient for the state estimate to converge.

C. Tracking Control Performance Using State Observer

In this section, the performance of the tracking controller is assessed when used in conjunction with the state estimator. The electrodynamic tether system is sensitive when operated at high currents, such as those used in these examples. An illustration of this can be seen by referring to Fig. 3b, which shows the rapid divergence of the system into a tumbling mode. Therefore, it is important to demonstrate that the feedback control architecture is still robust when used in a sampled-data, inexact state feedback context. In most of the previous work on electrodynamic tether control, full state feedback of the truth has been assumed.

The following example begins with the tether aligned with the local vertical. The orbit inclination is 45 deg, and the filter parameters are selected as previously. The nondimensional current is initially applied at the desired value of 1.5, and the feedback controller is initialized after the true anomaly is greater than 1 rad. The initial application of current simulates switching on the current and excites the system. The nondimensional current is bounded between 0 and 2 for this example.

Numerical results are shown in Fig. 6. Figure 6a shows the trajectory of the tether on the phase plane together with the reference periodic solution. The closed-loop solution converges to the reference trajectory after approximately 1.5 orbits, after which the reference solution is tracked with negligible tracking errors. This illustrates that all tether states do not need to be directly measured. The filtered state estimate is suitable for implementation in the sampled-data feedback architecture. The applied feedback control is shown in Fig. 6b. This shows that the current is initially at the desired value of 1.5 until the feedback controller is activated. The current initially saturates at 0, and then later saturates at the maximum of 2, before settling to the quasi-steady value of 1.5. The same fluctuations in the control current can be seen in Fig. 6b after the trajectory has converged. This is due to the inexact reference solution. A comparison of Fig. 6b with Fig. 4b shows that it takes longer and more variation in the current to stabilize the tether in this example. This is due to the larger initial errors in the tether state when the controller is activated than in the previous example.

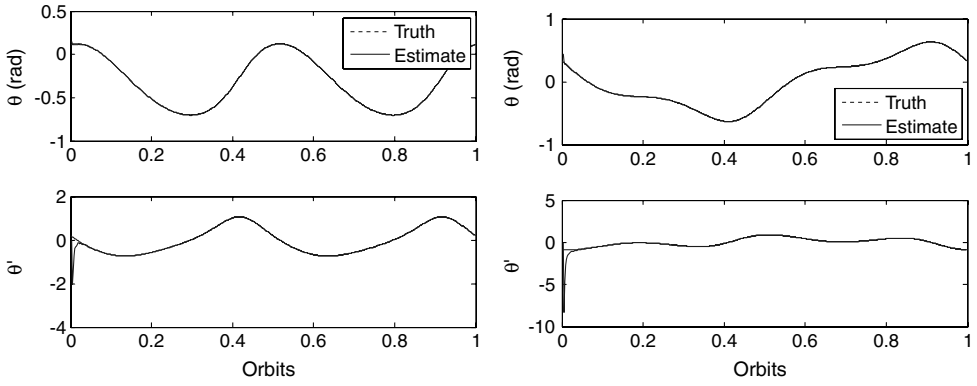

Fig. 5 Convergence of state estimates to true solution.

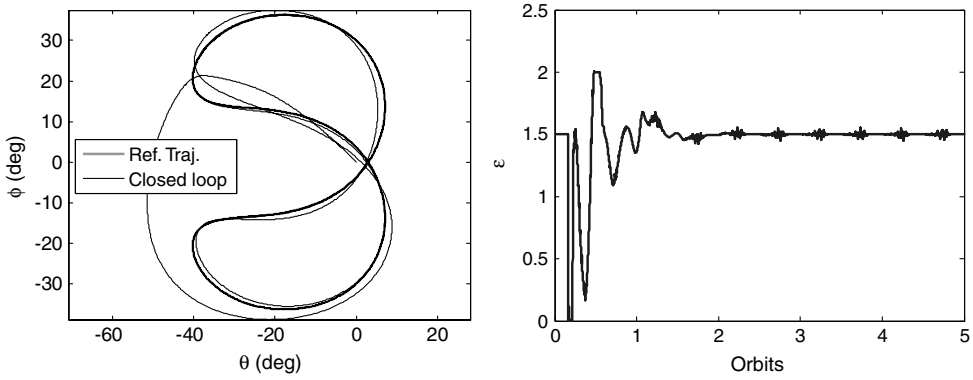

a) b)

Fig. 6 a) Convergence of electrodynamic tether to reference trajectory with inexact state feedback starting from zero libration; b) applied nondimensional current for tracking of reference trajectory with feedback of state estimates.

D. Time-Delayed Predictive Control: Circular Orbit Case

In this example, the convergence of the time-delayed predictive controller is demonstrated for the simple case of a circular orbit. This implies that the orbital parameters remain fixed. The system begins at the local vertical for one orbit before the delayed-feedback controller starts. The control input is limited to the range $1 \leq \varepsilon \leq 2$. The forward prediction horizon is one-half an orbit, and the backward time delay is one orbit. The sampling time for the control is equal to 0.25 rad, which is approximately 225 s for a low Earth orbit. The weighting matrices for penalizing deviations from the measured trajectories on the previous orbit are selected as $\mathbf{Q} = \mathbf{I}_{4\times4}$, and $R = 1$.

Figure 7a shows the evolution of the libration dynamics over a period of 400 orbits. Starting from rest, it is clear that the system moves into a periodic orbit after a long enough time. This represents convergence from a state which is very far from the desired one. The trajectory converges to the true periodic solution, which is shown in Fig. 7b. Figure 7b shows the periodic trajectory for the same orbit together with the closed-loop solution generated via time-delayed predictive control (TDPC). The TDPC solution is shown for the final orbit of the simulation. Figure 7b shows very good agreement between the numerically derived periodic solution and the one obtained without a priori knowledge of the solution. This illustrates the applicability of the TDPC scheme for stabilizing the librational motion of electrodynamic tethers.

Figure 8a shows the feedback control of the nondimensional current that stabilizes the periodic motion. The control saturates at the limits during the initial 20 orbits but converges to the desired mean of 1.5. It is interesting to note that a similar phenomenon in the control is observed as in the case of pure tracking control, that is, the control is not static, but varies by approximately ± 0.05. The control input shown in Fig. 8a appears exaggerated due to the scale of the axes. Figure 8b shows a close-up of the control between orbits 385 and 390. This shows that the fluctuations in control are only minor, and the current is generally constant during the periodic motion.

As a comparison, the case where the state measurements are obtained via the unscented filter is used to examine the effects of inexact state feedback. The state measurements are used for both the initial state in the predictive controller, as well as for the trajectory measured over the previous orbit. In the latter case, the filtered states are interpolated at the discrete sampling points used in the predictive controller by way of cubic splines.

Figure 9a shows the difference in the in-plane libration angle between the case where the true libration state is used and where the estimate is used. It is important to point out that this is the difference in the true feedback-controlled solutions between the two cases, not the difference between the estimated angle and the true angle. The results show that the use of filtered state estimates produces only a maximum difference of approximately 0.1 deg. Figure 9b shows the difference in the solutions for the out-of-plane angle. In this case, the maximum difference is approximately 0.15 deg. These results clearly illustrate that the system is able to function using inexact feedback and inexact measurements of the trajectories over the previous orbit for stabilization.

E. Time-Delayed Predictive Control: Elliptical Orbit Case

In the following example, the case of an elliptical orbit is considered. The orbit evolves from a circular orbit to one with an eccentricity of 0.2 in 100 orbits. The tether is initially aligned with the local vertical with no applied current. When the controller is applied, the control input is limited to the range $1 \leq \varepsilon \leq 2$. All other parameters are the same as in the previous example.

Figure 10a shows the results from the TDPC for a period of 400 orbits. Comparing Fig. 10a with Fig. 7a illustrates that orbit eccentricity has a significant effect on the libration dynamics. In this

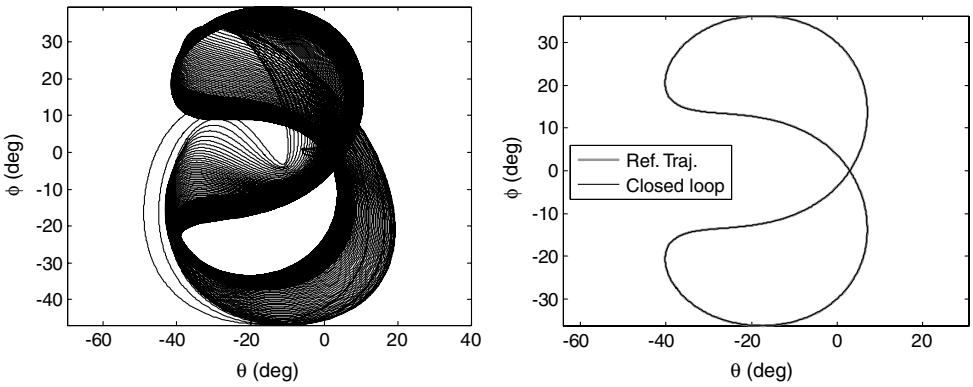

a) b)

Fig. 7 a) Evolution of electrodynamic tether librations over 400 orbits starting from rest with time-delayed predictive control; b) final orbit of electrodynamic tether librations stabilized using time-delayed predictive control.

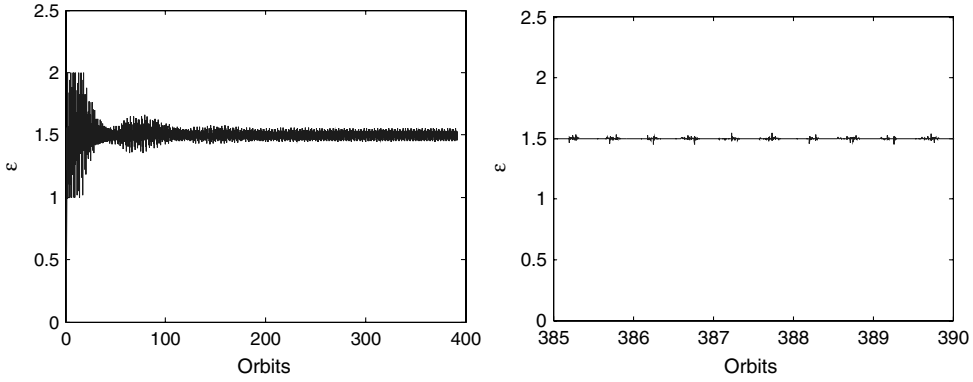

a) b)

Fig. 8 a) Feedback control generated using time-delayed predictive control over 400 orbits; b) close-up of feedback control for five orbits.

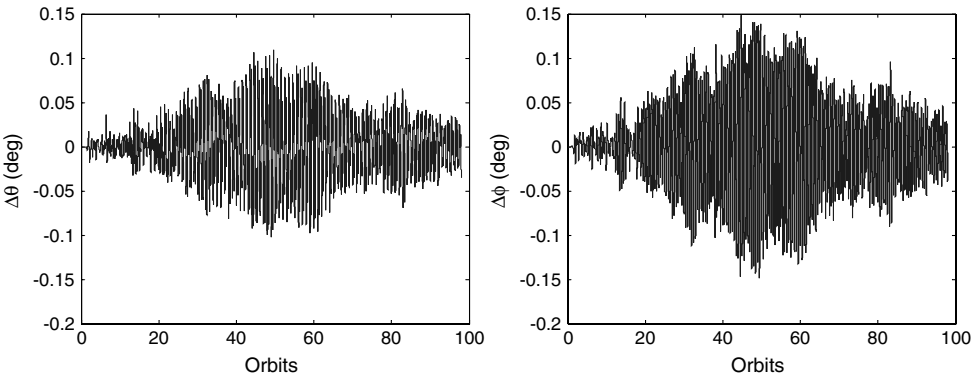

a) b)

Fig. 9 a) Effect of using state estimates on in-plane libration angle showing difference with solution generated using true states; b) effect of using state estimates on out-of-plane libration angle showing difference with solution generated using true states.

case, both the eccentricity and electrodynamics are forcing functions to the librations. The orbit eccentricity creates a destabilizing effect on the periodic solution. However, TDPC stabilizes the periodic motion, as shown in Fig. 10b. The applied current is shown in Fig. 11, which shows that the librations have not completely converged to a solution with constant applied current. However, in practice, the orbit of the system is continually changing under the application of electrodynamic forces. Therefore, the important property of the controller is that it keeps the librations bounded with a current that is maintained close to the desired current.

F. Time-Delayed Predictive Control: Sinusoidal Current Demand

The previous examples considered the case of a constant reference current. In this example, a sinusoidal reference current is used of the form

$$\varepsilon_r = \sin 2\nu \tag{75}$$

which can be used for rotating the longitude of the ascending node of an orbit. To keep the control input from significantly deviating from the reference current, it is bounded using a time-varying path constraint

$$-0.5 + \sin 2\nu \leq \varepsilon \leq 0.5 + \sin 2\nu \tag{76}$$

All other parameters are kept the same as the previous examples. Numerical results are shown in Fig. 12. In [37], it was shown that some forced current profiles have stable periodic solutions for some inclinations and current amplitudes. The results shown in Fig. 12a

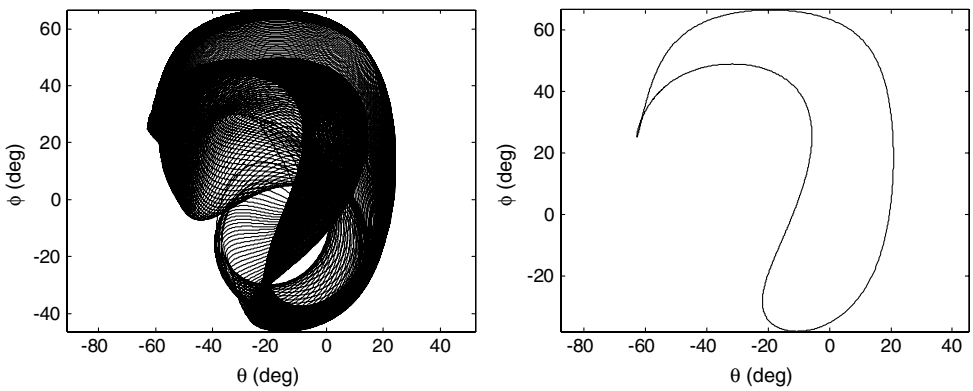

a) b)

Fig. 10 a) Evolution of electrodynamic tether librations over 400 orbits with time-delayed predictive control in elliptic orbit, $e = 0.2$; b) stabilized periodic solution using time-delayed predictive control with $e = 0.2$, orbit 400.

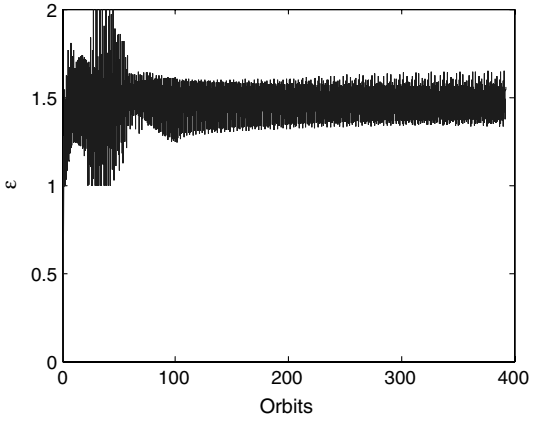

Fig. 11 Feedback control generated using time-delayed predictive control over 400 orbits for $e = 0.2$.

suggest that the periodic solution is indeed stable because of the fast convergence to a periodic trajectory. The system is initially aligned with the local vertical, but converges to a trajectory that is close to the final one in approximately 10 orbits. The variation in current required to achieve this is best viewed as the difference between the applied and the desired current, as shown in Fig. 12b. This shows that initially no current is applied and the error is equal to the desired current. The rapid convergence of the current is evident in Fig. 12b, but small corrections are required for approximately 50 orbits.

G. Time-Delayed Predictive Control: Orbit Decay Dynamics, Nontilted Dipole

The previous examples demonstrate the wide applicability of the time-delayed predictive control strategy for the electrodynamic tether. The real test of the controller, however, is whether it stabilizes the librations during orbital maneuvers. One of the most important maneuvers is deorbit [10,11]. Deorbiting by means of electrodynamic tethers can potentially reduce costs associated with launching satellites because of the lower propellant requirements. Hence, the purpose of this example is to demonstrate the controller in the case where the electrodynamic tether system deorbits according to the forces generated.

The system is initially placed in a 500 km altitude orbit with an eccentricity of 0.02. The small eccentricity is required to prevent the singularity in the perturbation equations presented in Sec. II. It should be noted, however, that the use of the perturbation equations in no way restricts applicability of the controller. The perturbation equations are only used to simulate the orbit evolution of the tether system. The argument of perigee is initially zero and the right ascension of the ascending node is also initially zero. The orbit inclination is initially 45 deg. In this first example, the magnetic field is assumed to be modeled using a nontilted dipole.

For simulation of the orbital dynamics, it is necessary to dimensionalize the system. The tether length is 5 km, the main satellite is 1000 kg, the ballast mass is 50 kg, and the tether mass is 40 kg. These values are used to convert the nondimensional current into a dimensional one via Eq. (23), which is used in the calculation of the Lorentz forces for deorbiting. It is important to point out, however, that the current is assumed to be available independently of the ionospheric conditions. No effort has been made in the current work to incorporate a realistic model of current collection. Using such a model, it would be possible to use more appropriate time-varying bounds on the nondimensional current used in the control law. Instead, the tether has been sized approximately to achieve the current required by the control law, assuming a high plasma density. Additionally, a power supply would be required to boost the current in adverse operating conditions.

Numerical results for the tether librations are shown in Fig. 13a for a 200 orbit simulation. However, only the results where the system is above the surface of the Earth are shown. The results show that the controller has stabilized the tether librations to a trajectory that is very close to the periodic one on a frozen orbit. The trajectories on the phase plane are closely spaced for the majority of the orbits, indicating the effectiveness of the controller for handling the variation in all orbital elements. Figure 13b shows the applied current during the deorbit. There are no significant differences seen in this plot as compared to Fig. 8a for a frozen Keplerian orbit. The control corrections are generally quite small around the desired reference current.

Figure 14a shows the variation in orbital altitude of the system during deorbit. The altitude is reduced by 500 km after 166 orbits by application of the controller. The altitude drops in nearly a linear fashion, although there are short-term fluctuations over each orbit. Note that no atmospheric effects are included in the simulation, which would help to speed up the deorbit process at lower altitudes. Figure 14b shows the variation in the orbit eccentricity and inclination during the deorbit. It can be seen that the eccentricity remains relatively constant, but that the inclination increases by over 2 deg. To generate close to a pure deorbit force, that is, one that maintains constant orbit inclination, requires the application of a more complex reference current, which has been discussed in [16]. The current in this example is quite high for a deorbiting electrodynamic system ($\sim$10 A), and further work is needed to incorporate a realistic model of electron collection. Nevertheless, these results clearly demonstrate the effectiveness of the proposed controller for suppressing the librational instabilities at high currents. The libration dynamics are kept bounded and close to periodic, while simultaneously keeping the current close to the desired value.

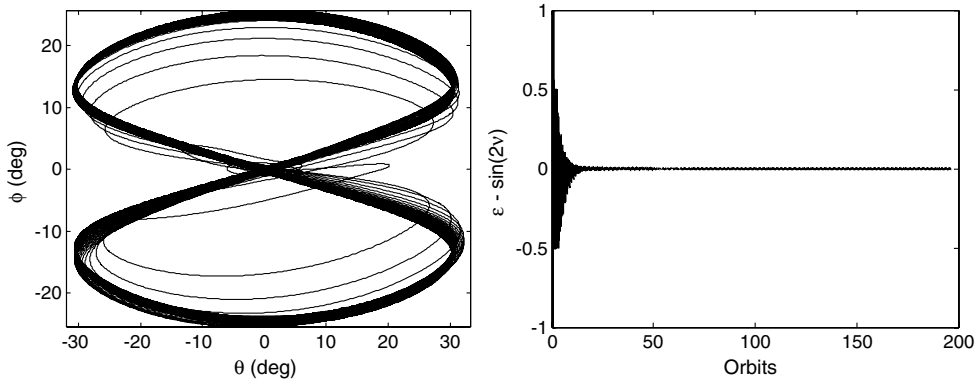

Fig. 12 a) Evolution of electrodynamic tether librations over 200 orbits with time-delayed predictive control in circular orbit and sinusoidal demanded current; b) convergence of applied current to desired current for sinusoidal demand.

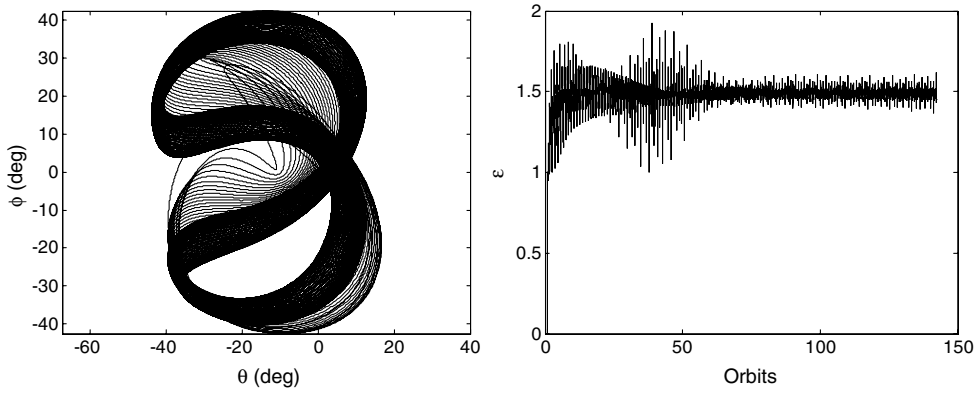

a) b)

Fig. 13 a) Evolution of electrodynamic tether librations during orbit decay over 200 orbits with time-delayed predictive control; b) feedback control generated using time-delayed predictive control during orbit decay.

H. Time-Delayed Predictive Control: Orbit Decay Dynamics, Tilted Dipole Model

In this final example, the time-delayed predictive controller is applied to the same deorbit problem, but the magnetic field is modeled using the tilted dipole representation. This introduces several effects that were not included previously. First, a tilted dipole representation does not give rise to natural periodic solutions due to the variation of the magnetic field orientation with the rotation of the Earth. This means that the controller cannot converge to a solution that does not involve control "corrections." Second, the rotation of the magnetic field with the Earth introduces an additional periodic effect on the Lorentz forces with a period that is a function of orbital speed and Earth's rotational period. In addition, in this example, the controller is applied using both true state feedback and feedback of the filtered state estimates. In the case where the state estimates are used, the variations of the orbital elements are not used in the predictive controller, that is, they remain constant over the prediction horizon. The same parameters are the same ones used in the deorbit with the nontitled dipole example. The deorbit is assumed to begin at midnight on 31 December 2006.

Figure 15a shows the results of the tether librations during deorbit with the tilted dipole. The forcing effect of the rotation of the magnetic field is evident by comparing Fig. 15a with Fig. 13a. The results show that the librations are kept bounded and "close" to

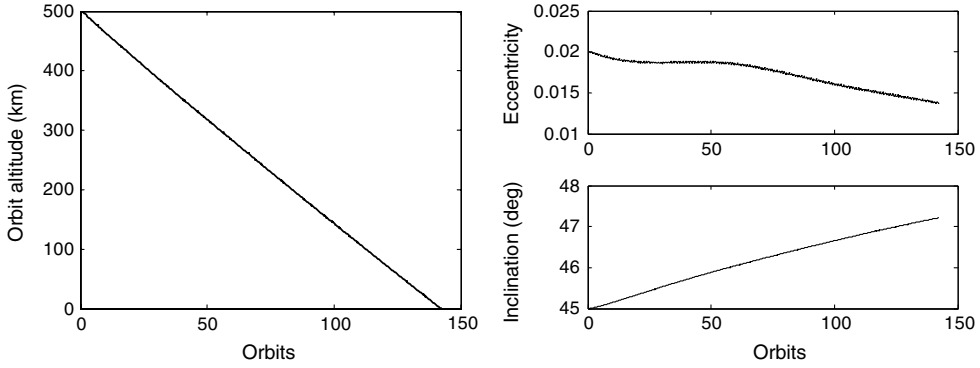

a) b)

Fig. 14 a) Orbit altitude of electrodynamic tether system during deorbit with nontilted dipole model; b) orbit eccentricity and inclination during deorbit with nontilted dipole model.

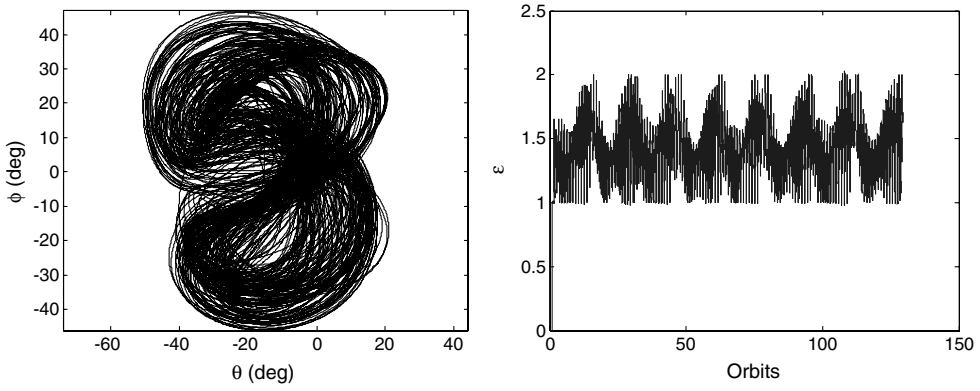

a) b)

Fig. 15 a) Evolution of electrodynamic tether librations during orbit decay over 200 orbits with time-delayed predictive control with tilted dipole model; b) applied nondimensional current during deorbit with tilted dipole.

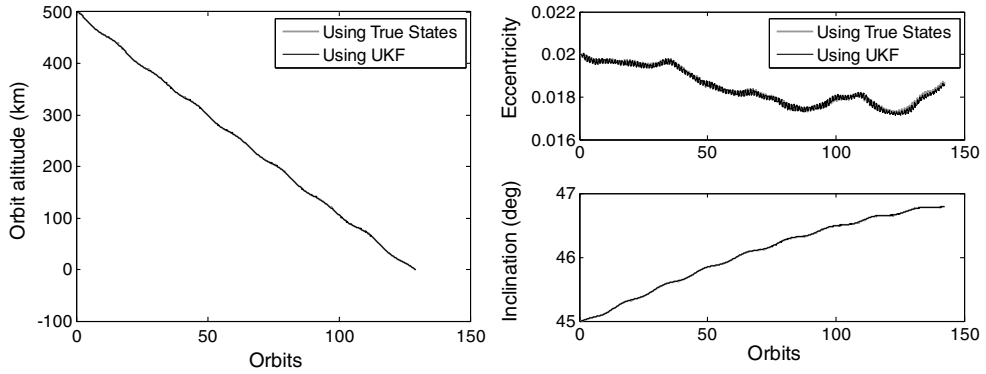

Fig. 16 a) Orbit altitude of electrodynamic tether system during deorbit with tilted dipole model showing a comparison of solutions generated with and without true states; b) orbit eccentricity and inclination during deorbit with tilted dipole model showing a comparison of solutions generated with and without true states.

periodic. Because the variation in orbital elements is similar to the nontilted dipole case, the variation in the trajectories on the phase plane is due mainly to the rotation of the magnetic field. Figure 15b shows the applied current during the deorbit with a tilted dipole. The current varies over a wider range during the entire deorbit. The periodic effect of the change in the magnetic field is evident by the shift in the mean value of the applied current. This contrasts with the nontilted dipole case, which followed the mean desired current value very well. The change in the magnetic field vector also produces a destabilizing effect, which requires more "effort" from the controller. It should be noted that an open-loop simulation of the reference current of $\varepsilon = 1.5$ becomes unstable after one orbit and commences rotating, making the deorbit infeasible without feedback control at such high currents.

Figure 16a shows the change in altitude during the deorbit, together with a comparison of the deorbit using filtered state estimates. The variation in altitude is approximately linear as in the case of a nontilted dipole, but there is an additional low frequency variation. This is the effect of the shift in the magnetic field. The rate of deorbit is faster in the tilted dipole case than in the nontilted case. This can be attributed to the fact that the direction of the deorbit forces are more closely aligned with the orbit direction in the case of a tilted dipole. This is confirmed by examining Fig. 16b, which shows the variation in eccentricity and inclination during the deorbit. The change in orbit inclination is approximately 1.65 deg compared with 2.1 deg for the nontilted case. Hence, less of the electrodynamic forces are directed normal to the orbit plane in the case of a tilted dipole. The eccentricity also stays closer to a constant value for the tilted dipole deorbit than for the nontilted dipole case.

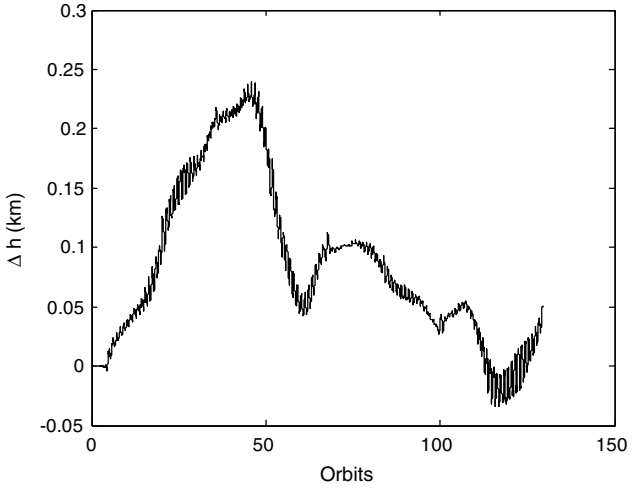

Fig. 17 Difference in orbital altitude between solution generated with true state feedback and feedback using filtered state estimates.

The effect of using filtered estimates on the accuracy of the deorbiting process is summarized in Fig. 17, which shows the difference in altitude produced as a result of using filtered estimates in the controller rather than the true values. The mean difference in altitude is approximately 100 m, but peaks to about 250 m after one-third of the deorbit. This difference can be considered negligible when compared with the total change in altitude, that is, 0.03–0.06% error. Hence, the controller is robust to inexact orbital parameters, state feedback, and periodic forcing functions caused by the tilted magnetic field.

V. Conclusions

A new control approach has been proposed for stabilizing electrodynamic tethers around their periodic solutions without a priori knowledge of the periodic solution. The approach has been termed time-delayed predictive control, which minimizes the predicted motion of the system over a future horizon from the motion measured during the previous orbit. The controller has been tested on a number of individual cases, including varying orbital parameters, elliptic orbits, forced reference currents, and system deorbit. Full parametric studies have not yet been undertaken to study the sensitivity of the controller. Feedback using filtered state estimates has also been demonstrated in individual examples. The control approach is able to stabilize the librations in the case where periodic solutions do not exist due to the rotation of the Earth's magnetic field. The controller is robust to inexact feedback created by estimating the tether dynamic state and shows great promise for further study.

Appendix: Magnetic Field Vector

The Earth's magnetic field can be approximated as a dipole for preliminary analysis. The following derivation is taken from [56], based on [22]. The general equation for the magnetic field vector modeled by a dipole is given by

$$\mathbf{B} = \frac{\mu_m}{r^3}(\mathbf{u}_m - 3(\mathbf{u}_m \cdot \mathbf{u}_r)\mathbf{u}_r) \tag{A1}$$

where μ_m is the dipole strength, $\mathbf{u}_m$ is the unit vector describing the orientation of the magnetic axis, and $\mathbf{u}_r$ is the unit position vector of the point of interest where the magnetic field vector is to be determined. Because the magnetic field is fixed in, and rotating with the Earth, it is convenient to define geographic reference axes which rotate with the Earth. This axis system is defined as shown in Fig. A1.

The geocentric inertial axes (X, Y, Z) are fixed at the center of the Earth, but do not rotate with it. The X axis is aligned with the vernal equinox, the Z axis is aligned in the direction of the north pole, and the Y axis completes the right-handed orthogonal triad. The geographic axis system (X_G, Y_G, Z_G) is fixed at the center of the Earth. The X_G axis is aligned with the Greenwich meridian, the

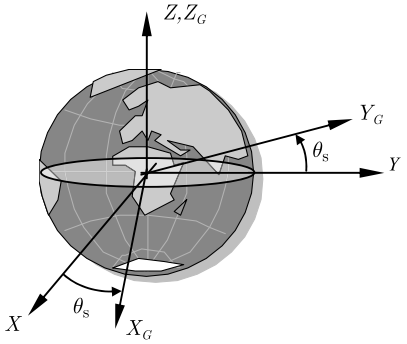

Fig. A1 Orientation of the geographic axis system.

Z_G axis is aligned in the direction of the north pole, and the Y_G axis completes the triad.

The magnetic dipole axis is located in the geographic axis system by the vector

$$\mathbf{u}_m = \sin\beta_m \cos\alpha_m \mathbf{X}_G + \sin\beta_m \sin\alpha_m \mathbf{Y}_G + \cos\beta_m \mathbf{Z}_G \quad \text{(A2)}$$

where α_m is the right ascension of the magnetic axis, and β_m is the dipole tilt of the magnetic axis from the axis of rotation. The values of α_m and β_m vary slowly with time, but the following representative values may be adopted: $\alpha_m = 256$ deg, and $\beta_m = 11.7$ deg.

The magnetic dipole axis vector in inertial coordinates is

$$\mathbf{u}_m = \sin\beta_m \cos(\theta_s(t) + \alpha_m)\mathbf{X} + \sin\beta_m \sin(\theta_s(t) + \alpha_m)\mathbf{Y} + \cos\beta_m \mathbf{Z} \quad \text{(A3)}$$

where $\theta_s(t)$ is the Greenwich sidereal time.

The magnetic dipole axis vector can be expressed in the local vertical-local horizontal coordinate system used to describe the tether dynamics by using the classical orbital elements, as shown in Fig. A2.

The orientation of the rotating coordinate system is given by a set of three Euler angle rotations in the sequence $C_3(\varpi) \leftarrow C_1(i) \leftarrow C_3(\Omega)$, where Ω is the right ascension of the ascending node, i is the inclination of the orbit plane, and ϖ is the argument of perigee. Applying the coordinate transformation, and noting that $\mathbf{u}_r = \mathbf{i}$ in the rotating coordinate system, the magnetic field vector may be determined as

$$B_x = -2\frac{\mu_m}{r^3}[\sin(\varpi+\nu)\sin i\cos\beta_m + \sin\beta_m\{\cos\lambda\cos(\varpi+\nu) + \sin\lambda\sin(\varpi+\nu)\cos i\}] \quad \text{(A4)}$$

$$B_y = \frac{\mu_m}{r^3}[\cos(\varpi+\nu)\sin i\cos\beta_m - \sin\beta_m\{\cos\lambda\sin(\varpi+\nu) - \sin\lambda\cos(\varpi+\nu)\cos i\}] \quad \text{(A5)}$$

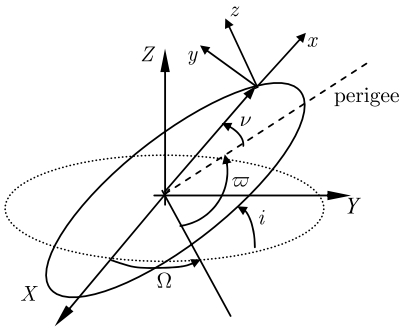

Fig. A2 Orientation of the local tether coordinate system relative to the inertial Earth coordinate system.

$$B_z = \frac{\mu_m}{r^3}[\cos i\cos\beta_m - \sin\beta_m \sin i\sin\lambda] \quad \text{(A6)}$$

where $\lambda = \alpha_m + \theta_s(t) - \Omega$. In some cases, it is assumed that the magnetic field is a nontilted dipole which can be modeled using the approximation $\beta \approx 0$, so that the magnetic field vector is given by

$$\bar{B}_x = -2\frac{\mu_m}{r^3}\sin(\varpi+\nu)\sin i \quad \text{(A7)}$$

$$\bar{B}_y = \frac{\mu_m}{r^3}\cos(\varpi+\nu)\sin i \quad \text{(A8)}$$

$$\bar{B}_z = \frac{\mu_m}{r^3}\cos i \quad \text{(A9)}$$

References

[1] Carroll, J. A., "Tether Applications in Space Transportation," *Acta Astronautica*, Vol. 13, No. 4, 1984, pp. 165–174. doi:10.1016/0094-5765(86)90061-5

[2] Rawer, K., "Tether Applications: Note on an Article by J. A. Carroll," *Acta Astronautica*, Vol. 15, No. 12, 1987, p. 1051. doi:10.1016/0094-5765(87)90030-0

[3] Longuski, J. M., Puig-Suari, J., and Mechalas, J., "Aerobraking Tethers for the Exploration of the Solar System," *Acta Astronautica*, Vol. 35, Nos. 2/3, 1995, pp. 205–214. doi:10.1016/0094-5765(94)00273-O

[4] Johnson, L., Estes, R. D., Lorenzini, E. C., Martinez-Sanchez, M., Sanmartin, J., and Vas, I., "Electrodynamic Tethers for Spacecraft Propulsion," AIAA Paper 98-9083, 1998.

[5] Forward, R., and Nordley, G., "Mars-Earth Rapid Interplanetary Tether Transport (MERITT) System: Initial Feasibility Analysis," AIAA Paper 99-2151, 1999.

[6] Moon & Mars Orbiting Spinning Tether Transport Architecture Study, Final Report on NIAC Phase II Contract 07600-034 with NASA Institute for Advanced Concepts, Universities Space Research Association, submitted by Tethers Unlimited, Inc., 31 Aug. 2001.

[7] Williams, P., Blanksby, C., and Trivailo, P., "Tethered Planetary Capture Maneuvers," *Journal of Spacecraft and Rockets*, Vol. 41, No. 4, 2004, pp. 603–613. doi:10.2514/1.1024

[8] Johnson, L., Estes, R. D., Lorenzini, E. C., Martinez-Sanchez, M., Sanmartin, J., and Vas, I., "Electrodynamic Tethers for Spacecraft Propulsion," AIAA Paper 98-0983, Jan. 1998.

[9] Johnson, L., and Herrmann, M., "International Space Station Electrodynamic Tether Reboost Study," NASA Marshall Space Flight Center, NASA/TM-1998-208538, July 1998.

[10] Hoyt, R., "Tether Systems for Satellite Deployment and Disposal," International Astronautical Federation Paper 00-S.6.04, Oct. 2000.

[11] Forward, R. L., Hoyt, R. P., and Uphoff, C. W., "Terminator Tether: A Spacecraft Deorbit Device," *Journal of Spacecraft and Rockets*, Vol. 37, No. 2, 2000, pp. 187–196. doi:10.2514/2.3565

[12] Gallagher, D. L., Johnson, L., Moore, J., and Bagenal, F., "Electrodynamic Tether Propulsion and Power Generation at Jupiter," NASA Marshall Space Flight Center, NASA/TP-1998-208475, June 1998.

[13] Ishige, Y., Kawamoto, S., and Kibe, S., "Study on Electrodynamic Tether System for Space Debris Removal," International Astronautical Federation Paper 02-A.7.04, Oct. 2002.

[14] Yamagiwa, Y., Sakata, Y., and Hara, N., "Performance of Electrodynamic Tether Orbit Transfer System on the Orbit with Inclination," Japan Society for Aeronautical and Space Sciences, ISTS-00-k-24, 2000, pp. 1807–1812.

[15] Lanoix, E. L. M., Misra, A. K., Modi, V. J., and Tyc, G., "Effect of Electromagnetic Forces on the Orbital Dynamics of Tethered Satellites," American Astronautical Society Paper 00-189, 2000.

[16] Tragesser, S. G., and San, H., "Orbital Maneuvering with Electrodynamic Tethers," *Journal of Guidance, Control, and Dynamics*, Vol. 26, No. 5, 2003, pp. 805–810. doi:10.2514/2.5115

[17] Williams, P., "Optimal Orbital Maneuvering Using Electrodynamic Tethers," American Astronautical Society Paper 05-206, Jan. 2005.

[18] Williams, P., "Simple Approach to Orbital Control Using Spinning Electrodynamic Tethers," *Journal of Spacecraft and Rockets*, Vol. 43, No. 1, 2006, pp. 253–256. doi:10.2514/1.16608
[19] Williams, P., "Optimal Orbital Transfer with Electrodynamic Tether," *Journal of Guidance, Control, and Dynamics*, Vol. 28, No. 2, 2005, pp. 369–372. doi:10.2514/1.12016
[20] Pearson, J., Carroll, J., Levin, E., Oldson, J., and Hausgen, P., "Overview of the Electrodynamic Delivery Express (EDDE)," AIAA Paper 2003-4790, July 2003.
[21] Pearson, J., Levin, E., Carroll, J. A., and Oldson, J. C., "Orbital Maneuvering with Spinning Electrodynamic Tethers," AIAA Paper 2004-5715, Aug. 2004.
[22] Pelaez, J., Lorenzini, E. C., Lopez-Rebollal, O., and Ruiz, M., "A New Kind of Dynamic Instability in Electrodynamic Tethers," *Journal of the Astronautical Sciences*, Vol. 48, No. 4, 2000, pp. 449–476.
[23] Pelaez, J., and Lara, M., "Periodic Solutions in Electrodynamic Tethers on Inclined Orbits," *Journal of Guidance, Control, and Dynamics*, Vol. 26, No. 3, 2003, pp. 395–406. doi:10.2514/2.5077
[24] Williams, P., "Energy Rate Feedback for Libration Control of Electrodynamic Tethers," *Journal of Guidance, Control, and Dynamics*, Vol. 29, No. 1, 2006, pp. 221–223. doi:10.2514/1.17530
[25] Bleich, M. E., and Socolar, J. E. S., "Stability of Periodic Orbits Controlled by Time-Delay Feedback," *Physics Letters A*, Vol. 210, Nos. 1–2, 1996, pp. 87–94. doi:10.1016/0375-9601(95)00827-6
[26] Fujii, H. A., Ichiki, W., Suda, S., and Watanabe, T. R., "Chaos Analysis on Librational Control of Gravity-Gradient Satellite in Elliptic Orbit," *Journal of Guidance, Control, and Dynamics*, Vol. 23, No. 1, 2000, pp. 145–146. doi:10.2514/2.4500
[27] Pelaez, J., and Lorenzini, E. C., "Libration Control of Electrodynamic Tethers in Inclined Orbits," *Journal of Guidance, Control, and Dynamics*, Vol. 28, No. 2, 2005, pp. 269–279. doi:10.2514/1.6473
[28] Inarrea, M., and Pelaez, J., "Libration Control of Electrodynamic Tethers Using the Extended Time-Delayed Autosynchronization Method," American Astronautical Society Paper 07-194, Jan. 2007.
[29] Takeichi, N., "Libration Control of an Electrodynamic Tether System Through Electric Current Switching," American Astronautical Society Paper 05-318, Aug. 2005.
[30] Lorenzini, E. C., Bortolami, S. B., Rupp, C. C., and Angrilli, F., "Control and Flight Performance of Tethered Satellite Small Expendable Deployment System-II," *Journal of Guidance, Control, and Dynamics*, Vol. 19, No. 5, 1996, pp. 1148–1156. doi:10.2514/3.21757
[31] Zimmerman, F., Schöttle, U. M., and Messerschmid, E., "Optimal Deployment and Return Trajectories for a Tether-Assisted Re-Entry Mission," AIAA Paper 99-4168, Aug. 1999.
[32] Misra, A. K., and Modi, V. J., "A Survey on the Dynamics and Control of Tethered Satellite Systems," *Advances in the Astronautical Sciences*, Vol. 62, 1987, pp. 667–719.
[33] Fujii, H. A., and Anazawa, S., "Deployment/Retrieval Control of Tethered Subsatellite Through an Optimal Path," *Journal of Guidance, Control, and Dynamics*, Vol. 17, No. 6, 1994, pp. 1292–1298. doi:10.2514/3.21347
[34] Barkow, B., Steindl, A., Troger, H., and Wiedermann, G., "Various Methods of Controlling the Deployment of a Tethered Satellite," *Journal of Vibration and Control*, Vol. 9, No. 1, 2003, pp. 187–208. doi:10.1177/1077546303009001747
[35] Williams, P., "Spacecraft Rendezvous on Small Relative Inclination Orbits Using Tethers," *Journal of Spacecraft and Rockets*, Vol. 42, No. 6, 2005, pp. 1047–1060. doi:10.2514/1.11826
[36] Williams, P., "Nonlinear Control and Applications of Tethered Space Systems," Ph.D. Dissertation, RMIT University, Melbourne, Australia, 2004.
[37] Williams, P., "Periodic Solutions of Electrodynamic Tethers Under Forced Current Variations," AIAA Paper 2006-6765, 2006.
[38] Pelaez, J., "Self Balanced Electrodynamic Tether," AIAA 2004-5309, Aug. 2004.
[39] Walker, M. J. H., Ireland, B., and Owens, J., "A Set of Modified Equinoctial Orbit Elements," *Celestial Mechanics*, Vol. 36, No. 4, 1985, pp. 409–419. doi:10.1007/BF01227493
[40] Dunbar, W. B., Milam, M. B., Franz, R., and Murray, R. M., "Model Predictive Control of a Thrust-Vectored Flight Control Experiment," *15th IFAC World Congress on Automatic Control*, Elsevier, Oxford, 2002.
[41] Franz, R., Milam, M., and Hauser, J., "Applied Receding Horizon Control of the Caltech Ducted Fan," *Proceedings of the American Control Conference*, IEEE, Piscataway, NJ, 2002.
[42] Elnagar, G., Kazemi, M. A., and Razzaghi, M., "The Pseudospectral Legendre Method for Discretizing Optimal Control Problems," *IEEE Transactions on Automatic Control*, Vol. 40, No. 10, 1995, pp. 1793–1796. doi:10.1109/9.467672
[43] Ross, I. M., and Fahroo, F., "Legendre Pseudospectral Approximations of Optimal Control Problems," *New Trends in Nonlinear Dynamics and Control, and Their Applications*, edited by W. Kang, M. Xiao, and C. Borges, Vol. 295, Lecture Notes in Control and Information Sciences, Springer–Verlag, Berlin, 2003, pp. 327–342.
[44] Yan, H., Ross, I. M., and Alfriend, K. T., "Time-Optimal Magnetic Attitude Control Toward Real-Time Application," American Astronautical Society Paper 05-233, Jan. 2005.
[45] Williams, P., and Trivailo, P., "Optimal Motion Planning and Tracking Control for a Flexible Manipulator," *56th International Astronautical Congress*, Curran Associates, Inc., New York, IAC-05-C1.P.14, 17–21 Oct. 2005.
[46] Yan, H., Lee, D.-J., Ross, I. M., and Alfriend, K. T., "Real-Time Outer and Inner Loop Optimal Control using DIDO," American Astronautical Society Paper 05-353, Aug. 2005.
[47] Williams, P., "Real-Time Computation of Optimal Trajectories for Tethered Satellite Systems," American Astronautical Society Paper 05-320, 2005.
[48] Williams, P., "Application of Pseudospectral Methods for Receding Horizon Control," *Journal of Guidance, Control, and Dynamics*, Vol. 27, No. 2, 2004, pp. 310–314. doi:10.2514/1.5118
[49] Williams, P., "A Gauss-Lobatto Quadrature Approach for Solving Optimal Control Problems," *ANZIAM Journal (E)*, Vol. 47, July 2006, pp. C101–C115.
[50] Williams, P., and Trivailo, P., "Optimal Parameter Estimation of Dynamical Systems Using Direct Transcription Methods," *Inverse Problems in Science and Engineering*, Vol. 13, No. 4, 2005, pp. 377–409. doi:10.1080/17415970500104499
[51] Benson, D., "A Gauss Pseudospectral Transcription for Optimal Control," Ph.D. Dissertation, Massachusetts Institute of Technology, Boston, MA, Nov. 2004.
[52] Gill, P. E., Murray, W., and Saunders, M. A., "SNOPT: An SQP Algorithm for Large-Scale Constrained Optimization," *SIAM Journal on Optimization*, Vol. 12, No. 4, 2002, pp. 979–1006. doi:10.1137/S1052623499350013
[53] Julier, S. J., Uhlmann, J. K., and Durrant-Whyte, H., "A New Approach for Filtering Nonlinear Systems," *Proceedings of the American Control Conference*, IEEE, Piscataway, NJ, 1995, pp. 1628–1632.
[54] Williams, P., "Direct Numerical Computation of Periodic Orbits and Their Stability," *Journal of Spacecraft and Rockets*, Vol. 43, No. 5, 2006, pp. 1143–1146. doi:10.2514/1.20930
[55] Montenbruck, O., "LEO Satellite Navigation Errors in Single-Frequency GPS Tracking," Deutsches Zentrum für Luft- und Raumfahrt, Oberpfaffenhofen, DLR-GSOC TN 05-03, http://www.weblab.dlr.de/rbrt/pdf/TN_0504.pdf.
[56] Williams, P., Blanksby, C., and Trivailo, P., "The Use of Electromagnetic Lorentz Forces as a Tether Control Actuator," *53rd International Astronautical Congress*, Curran Associates, Inc., New York, IAC-02-A.5.04, 10–19 Oct. 2002.